THE JOURNAL OF PHYSICAL CHEMISTRY A

Article

pubs.acs.org/JPCA



# Explaining the Temperature Dependence of Spirilloxanthin's S* Signal by an Inhomogeneous Ground State Model

J. Hauer,[†,⊥] M. Maiuri,[‡,⊥] D. Viola,[‡] V. Lukes,[§] S. Henry,[∥] A. M. Carey,[∥] R. J. Cogdell,[∥] G. Cerullo,[‡] and D. Polli*[,‡]

[†]Photonics Institute, Vienna University of Technology, Gusshausstrasse 27, 1040 Vienna, Austria

[‡]IFN-CNR, Dipartimento di Fisica, Politecnico di Milano, Piazza L. da Vinci, 32, 20133 Milano, Italy

[§]Department of Chemical Physics, Slovak University of Technology, Radlinského 9, 81237 Bratislava, Slovakia

[∥]Institute for Molecular Biology, University of Glasgow, Glasgow G12 8TA, United Kingdom

**ABSTRACT:** We investigate the nature of the S* excited state in carotenoids by performing a series of pump−probe experiments with sub-20 fs time resolution on spirilloxanthin in a polymethylmethacrylate matrix varying the sample temperature. Following photoexcitation, we observe sub-200 fs internal conversion of the bright $S_2$ state into the lower-lying $S_1$ and S* states, which in turn relax to the ground state on a picosecond time scale. Upon cooling down the sample to 77 K, we observe a systematic decrease of the $S^*/S_1$ ratio. This result can be explained by assuming two thermally populated ground state isomers. The higher lying one generates the S* state, which can then be effectively frozen out by cooling. These findings are supported by quantum chemical modeling and provide strong evidence for the existence and importance of ground state isomers in the photophysics of carotenoids.

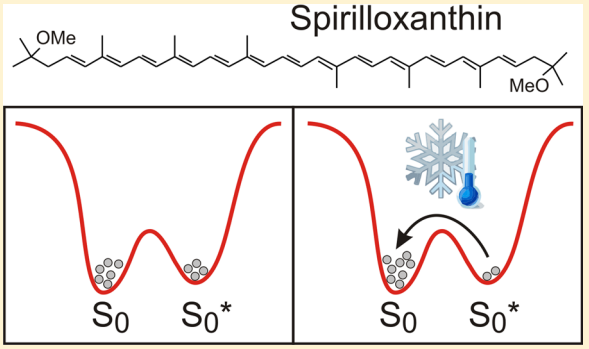


## INTRODUCTION

Carotenoids and chlorophylls are the two fundamental building blocks of natural light harvesting complexes. The role of carotenoids is 2-fold:[1] on one hand, they absorb and utilize sunlight in the blue−green spectral region; on the other hand, they photoprotect the light harvesting complex by quenching chlorophyll triplet- and oxygen singlet-states. Most of the remarkable properties of carotenoids can be explained by their delocalized $\pi$-electron system along their polyenic backbone. The lowest excited state in carotenoids, $S_1$, is dark with respect to the ground state due to symmetry reasons. The first optically allowed transition to $S_2$ is broad and shows strong vibronic modulation in the 18 200−25 000 $cm^{-1}$ region. After the initial excitation event, population transfer between $S_2$ and $S_1$ occurs on a sub-200 fs time scale. The excited state absorption (ESA) signal from $S_1$ is red-shifted compared to the ground state transition and exhibits the strongest transition dipole moment found in naturally abundant molecules. The electronic structure and energy deactivation pathways of carotenoids are a matter of ongoing debate.[2] Employed experimental methods range from sub-10 fs pump−probe,[3] fs-Raman,[4] four-wave-mixing methods,[5−10] electronic 2D-spectroscopy,[11−13] and several other techniques.[1,2] Despite such efforts, no consensus has yet been reached, as summarized in a review article by Polivka and Sundstrom.[2] The models proposed by different research teams deviate substantially in the interpretation of an electronic state named S*. S* manifests itself as a high-energy shoulder of the $S_1$-ESA band. Depending on the chain length of the investigated carotenoid, the S* lifetime can be substantially longer or on the same time scale as $S_1$. As first described for long-chain $\beta$-carotene homologues,[14] S* has been interpreted as a separate electronic excited state,[15−20] an excited state isomer,[21] a vibrationally hot ground state, populated by either Impulsive Stimulated Raman Scattering (ISRS)[22,23] or relaxation form $S_1$,[24,25] the product of different ground state isomers,[11,26,27] or as the result of chemical impurities.[28] We note that none of the proposed energy level models is able to explain all experimental findings in literature. For example: the fact that depletion of $S_2$ via an near-infrared (NIR)-pulse affects only $S_1$ but not S* has led to the hypothesis that S* stems from a vibrationally hot ground state (hot $S_0$), populated via an ISRS mechanism. However, experiments with varying excitation pulse bandwidth leave the S* signal unchanged,[29] which is not expected for ISRS-processes. Additionally, the hot ground state cannot be populated by the pump pulse in the linear regime of excitation. ISRS will rather produce coherence between $S_0$ and hot $S_0$ but will not populate hot $S_0$, as required for an ESA signal.[11] These problems are averted in a model where S* is populated after relaxation from $S_1$;[24] however, such an

**Special Issue:** Prof. John C. Wright Festschrift

**Received:** January 31, 2013
**Revised:** April 5, 2013
**Published:** April 11, 2013

   dx.doi.org/10.1021/jp4011372 | J. Phys. Chem. A 2013, 117, 6303−6310

assumption fails in explaining the ultrafast rise time of S*. If S* is assumed to be the product of an isomerization process on $S_1$,[21] the S* signal has again the correct ESA character and should be independent of temperature: in such a scenario, the activation energy for isomerization is not thermal, but provided by relaxation from $S_2$. This is in contrast to the observation of temperature effects on S*.[19,30] In a recent theoretical work, Lukes et al.[27] tried to combine all these findings in a model based on an inhomogeneous ground state. Briefly, the authors interpreted S* and $S_1$ as the lowest lying excited states of two stable ground state conformers. Such a model correctly predicts the properties of all pump−probe signals and their temperature dependence. Additionally, pump−deplete−probe results[22] can be explained assuming that the $S_2$ spectra of these two isomers differ; an NIR depletion pulse may then selectively deplete only one of them. Lukes et al.[27] showed that rotation of one of the end-groups of $\beta$-carotene is a promising candidate for the origin of such inhomogeneities. It was demonstrated that $\beta$-carotene's electronic ground state surface shows two thermally populated minima, where the global minimum is slightly asymmetric across the inversion center of the molecule, and the higher lying isomer shows $C_{2h}$ symmetry. It is interesting to note here that the ground state bleach (GSB) signal of carotenoids after the relaxation of $S_1$ but before depopulation of S* was reported to be more symmetric and more structured than the absorption spectrum.[31,32] It was therefore speculated that S* might stem from a subset of molecules showing higher symmetry than the $S_1$-forming ensemble. The higher lying isomer found upon end-group rotation with its $C_{2h}$ symmetry is a promising candidate for such a planar S*-forming subset.[27]

In this work, we put the inhomogeneous ground state hypothesis to a crucial test: if there are indeed two thermally populated ground state isomers (the energetically lower one forming $S_1$ and the other forming S*), then a decrease in temperature should enhance the ESA-signal from $S_1$ with respect to the signal associated with S*. Accordingly, we performed a series of pump−probe experiments at variable temperature on spirilloxanthin, which is the longest naturally occurring carotenoid, with 13 conjugated double bonds. To provide similar environments at any temperature ranging from room temperature (293 K, RT) down to liquid nitrogen (77 K), we could not dissolve spirilloxanthin in a solvent: we instead dispersed it in a polymethyl-methacrylate (PMMA) matrix, which is solid also at room temperature and does not change the observed dynamics with respect to liquid phase measurements. We conducted pump−probe experiments using ultrashort visible pump and probe pulses, with an overall sub-20 fs time resolution. We show that the $S^*/S_1$ ratio is indeed susceptible to temperature changes. Our findings, supported by quantum chemical modeling, provide strong evidence for the existence and importance of thermally populated ground state isomers in the photophysics of carotenoids.

## MATERIALS AND METHODS

**Synthesis.** Sprilloxanthin was extracted from *Rhodospirillum rubrum* cells grown anaerobically in the light in C-succinate media.[33] Cells were harvested and chromatophores prepared as described previously.[34] Membranes were suspended in acetone, stirred, and centrifuged at 429 × *g* for 3 min at 4 °C. The supernatant was discarded, and the pellet suspended in methanol, stirred, and centrifuged as before. This step was repeated until the majority bacteriochlorophyll *a* had been extracted (evident by the absence of blue in the pellet). Pellets were then resuspended in acetone, stirred, and centrifuged again at 429 × *g* for 3 min at 4 °C. This step was repeated until all carotenoid had been extracted from the pellet. The acetone/carotenoid mixture was then added to a separating funnel and mixed with a half volume of PET ether (40:60 b.p.) followed by an excess volume of warm, salty water. Carotenoids preferentially partitioned into the PET ether layer, which was collected and evaporated to dryness using a rotary evaporator. The dried carotenoid mixture was then redissolved in a small volume of PET ether and applied to an alumina (Merck, Aluminum Oxide 90) column. Carotenoids were separated using alumina column chromatography with an increasing gradient of diethyl ether in PET ether (modified from previously published methods).[35] Spirilloxanthin eluted at 30% diethyl ether and was identified by UV absorption spectroscopy on a Shimadzu 1700 spectrophotometer (Shimadzu, U.K.). Spirilloxanthin samples were pooled, dried under $N_2$, and redissolved in toluene. PMMA was dissolved in an equal quantity of toluene (w/v). The spirilloxanthin sample was then mixed with an equal volume of the PMMA solution, and 200 $\mu$L of this mixture was added to a 200 $\mu$m thick fused silica microscope slide. Slides were dried in a vacuum desiccator. The final OD of the dried samples ranged between 0.1 and 0.6 as measured by UV absorption spectroscopy. The actual sample studied in this work had OD = 0.15 at 540 nm, which is the excitation central wavelength. Carotenoid extractions and preparation of PMMA slides were performed in near darkness. Purity of the sample was confirmed by high performance liquid chromatography (HPLC).

**Ultrafast Spectroscopy.** The high time resolution experimental apparatus is based on two synchronized noncollinear optical parametric amplifiers (NOPAs),[36] pumped by a regeneratively amplified mode-locked Ti:Sapphire laser system delivering pulses with 150 fs duration, 500 $\mu$J energy, 1 kHz repetition rate, and 780 nm central wavelength. The first NOPA generates 15 fs pulses peaked at 540 nm (Pump in Figure 1), in resonance with the $S_0 \rightarrow S_2$ transition of spirilloxanthin. The second NOPA provides ultrabroadband

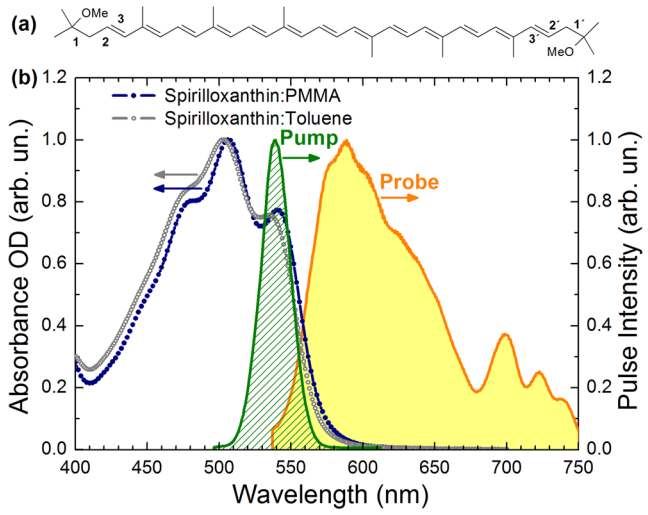


**Figure 1.** (a) Molecular structure of spirilloxanthin. (b) Normalized absorption spectrum of spirilloxanthin in toluene (gray circles) and PMMA matrix (blue circles) and pulse intensity spectra used in the experiment: the pump pulse (green shaded) and the probe pulse covering the visible (Probe, yellow area).


dx.doi.org/10.1021/jp4011372 | J. Phys. Chem. A 2013, 117, 6303−6310

probe pulses with ~7 fs duration spanning the 500−700 nm wavelength range (yellow filled spectrum in Figure 1). Both NOPAs are compressed to their transform-limited duration by multiple bounces on custom-designed chirped mirrors. The beams are focused onto the sample contained in a liquid nitrogen cryostat with 200 $\mu$m thick fused-silica entrance window. After the sample, the probe beam is selected by an iris and focused onto the entrance slit of a spectrometer with single-shot detection capability at 1 kHz.[37] Recording of the probe spectrum with and without the pump pulse, one can obtain the differential transmission ($\Delta T/T$) spectrum, defined as $\Delta T/T(\lambda,\tau) = [T_{on}(\lambda,\tau) - T_{off}(\lambda)]/T_{off}(\lambda)$, as a function of probe wavelength $\lambda$ and pump−probe delay $\tau$.

**Data Analysis.** For each sample temperature, we analyzed the measured two-dimensional $\Delta T/T$ maps using a homemade target analysis software, based on the approach described by van Stokkum et al.[38] We employed a kinetic scheme with 4 components ($S_2$, hot $S_1$, $S_1$, and S*) and 5 rate constants (named $k_1$−$k_5$), resulting in the estimated species associated difference spectra (SADS). In order to take into account the sharp features around time zero due to coherent artifacts such as cross-phase modulation, we also introduced two additional components with a delta-like (less than 5 fs duration) temporal evolution. The concentration profiles (and the above-mentioned components associated with the coherent artifacts) were convoluted with the instrument response function, which was fitted to a Gaussian of 18 fs duration (full width at half-maximum).

**Quantum Chemical Methods.** The B3LYP and/or BHLYP (Becke's half and half exchange functional with the LYP correlation functional) density functionals were applied in the Density Functional Theory (DFT) calculations of optimal electronic ground state geometries. The B3LYP functional includes Becke's three parameter mixing of the nonlocal exchange potential and the nonlocal correlation functional LYP proposed by Lee, Yang, and Parr.[39,40] On the basis of the optimized geometries, the electronic transitions were calculated using the time-dependent (TD)-DFT,[41] ab initio Complete Active Space Self-Consistent Field (CAS-SCF),[42] and Multi-reference Configuration Interaction (MRCI)[43] methods. In the ab initio multideterminant approaches, all valence electrons were correlated, and the reference space generation started by allowing all single and double excitations from the three highest occupied molecular orbitals to the three lowest unoccupied molecular orbitals. All quantum chemical calculations were performed with the ORCA 2.9.1 package.[44] We employed the split valence basis sets SV(P)[45,46] with a polarization d-function on carbon and oxygen atoms. The combination of the B3LYP functional with SV(P) or SVP basis sets offers a reliable description of torsional barriers, energy minima, and optimal geometries as demonstrated for various organic molecules.[47−49]

## RESULTS

Figure 2 shows experimental two-dimensional $\Delta T/T$ maps for spirilloxanthin in PMMA at RT (a) and at 77 K (b). In both cases, the pump wavelength (540 nm) was tuned to the red of the $S_0$−$S_2$ absorption, in order to minimize vibronic relaxation effects. We observe at early times a positive signal (in the high-energy part of the spectrum, red in Figure 2), which is assigned to the superposition of GSB (for wavelengths shorter than ~560 nm) and of stimulated emission (SE, for wavelengths longer than ~560 nm) from the $S_2$ state. The $\Delta T/T$ signal rapidly changes in sign to form, within ~500 fs, a broad ESA

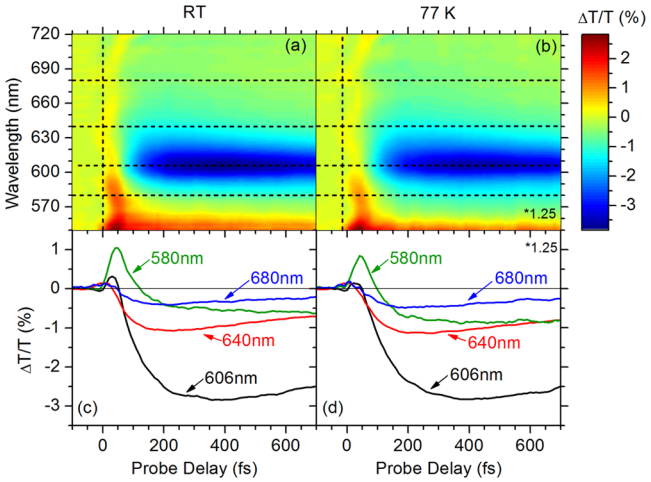


**Figure 2.** $\Delta T/T$ maps for spirilloxanthin as a function of probe wavelength and delay at room temperature (a) and at 77 K (b). Time traces at selected probe wavelengths (c,d). Excitation was at 540 nm.

band (ESA1, blue area in Figure 2 peaking at ~606 nm) that is assigned to the $S_1$−$S_n$ transition. This band narrows and blue-shifts on a longer time scale. The ESA1 band then decays on a picosecond time scale (outside the measurement window shown in Figure 2).

The observed photoinduced dynamics were fitted using the target analysis procedure detailed in the Materials and Methods section. Both at RT and at 77 K, it was possible to satisfactorily reproduce the data using four excited states: $S_2$, hot $S_1$, $S_1$, and S*, according to the energy level scheme shown in Figure 3a.

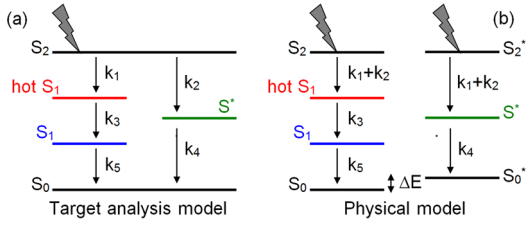


**Figure 3.** (a) Energy level scheme for spirilloxanthin used in the target analysis model to fit the temperature-dependent transient absorption spectra. (b) Inhomogeneous ground state model introduced to explain the temperature dependence of the signals.

Figure 3b shows the physical energy-level scheme, according to the inhomogeneous ground state model: two separate ground state isomers ($S_0$ and $S_0$*), energetically separated by $\Delta E$, are excited to their respective optically allowed states ($S_2$ and $S_2$*). Consequently, $S_2$ and $S_2$* decay to hot $S_1$ and S*, respectively. In our target analysis, we found that the model in Figure 3a suffices to explain our measurements, i.e., a common $S_2$ state branches to give hot $S_1$ and S*. If $S_2$ and $S_2$* are similar in both their SADS and decay time constants ($k_1 + k_2$ in Figure 3b), the two models in Figure 3 become mathematically equivalent. This is why we chose the simpler model in Figure 3a for the target analysis described below.

The extracted SADS are shown in Figure 4. Let us first discuss the RT results (Figure 4a). The first SADS can be identified as the $S_2$ state of spirilloxanthin and shows clear features of SE, i.e., the spectral positions of the vibronic replicas with mirror symmetry with the respective absorption bands. At the blue tail of the spectrum (wavelengths shorter than


dx.doi.org/10.1021/jp4011372 | J. Phys. Chem. A 2013, 117, 6303−6310

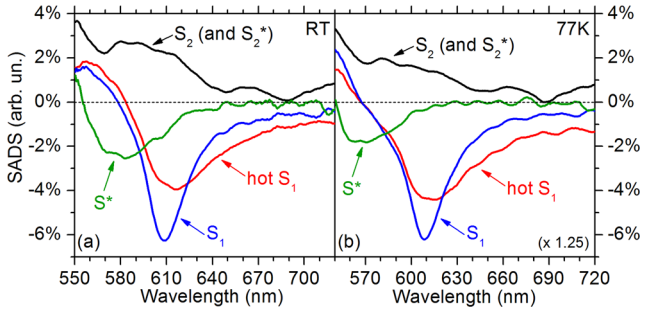


**Figure 4.** SADS extracted for spirilloxanthin in PMMA at room temperature (a) and at 77 K (b).

~560 nm), GSB also contributes to this SADS. From the $S_2$ state, two states are populated: hot $S_1$ and S*. Hot $S_1$ evolves with ~180 fs time constant into the relaxed $S_1$ state, which subsequently decays to the ground state with a 1.2 ps time constant. The S* state, however, decays to the ground state with a significantly slower time constant of 4.4 ps. The overall rates extracted from global analysis are shown in Table 1 and

**Table 1. Rate Constants Extracted from the Global Analysis of the $\Delta T/T$ Maps in Spirilloxanthin at RT and at 77 K**

| | $k_1$ | $k_2$ | $k_3$ | $k_4$ | $k_5$ |
|---|---|---|---|---|---|
| RT | (98 fs)$^{-1}$ | (196 fs)$^{-1}$ | (184 fs)$^{-1}$ | (4.4 ps)$^{-1}$ | (1.2 ps)$^{-1}$ |
| 77 K | (127 fs)$^{-1}$ | (254 fs)$^{-1}$ | (190 fs)$^{-1}$ | (8.9 ps)$^{-1}$ | (1.5 ps)$^{-1}$ |

are in good agreement with those we derived from a reference measurement of spirilloxanthin solvated in toluene under the same experimental conditions (not reported here) and with previous ultrafast spectroscopy studies of spirilloxanthin.[30,32,50−52]

When moving to 77 K, the SADS look qualitatively the same (see Figure 4b), with the spectral signatures of $S_2$, hot $S_1$, $S_1$, and S* clearly recognizable and very similar to those found at RT. However, by a closer inspection of the results, two significant differences become apparent: (i) The overall dynamics becomes slower at 77 K (see Table 1), with the rate constants for the internal conversion processes decreasing by 10 to 20%; this is in agreement with previous studies of carotenoids at cryogenic temperatures[19,30] and can be explained by the temperature dependence of system−bath interactions.[53] (ii) The relative weight of the S* and $S_1$ SADS changes upon cooling the sample; in particular, the parameter $r(T) = ((\int ESA_{S*}(\lambda,T)d\lambda)/(\int ESA_{S1}(\lambda,T)d\lambda))$, defined as the ratio of the integrals of the S* and $S_1$ SADS (limited to the negative portions of the spectra), decreases from $r$(RT) = 0.5 to $r$(77K) = 0.25. Assuming that the absorption cross-sections do not change significantly with temperature, this suggests that the relative weight (spectral amplitude) of the S* state decreases at 77 K, i.e., that the state is frozen out.

To confirm this last finding, we performed a systematic series of measurements varying the sample temperature from 77 K to RT and acquiring, for each temperature, the $\Delta T/T$ map. By performing the same target analysis on all the retrieved maps, we could extract the temperature dependence of the parameter $r(T)$, which is shown in Figure 5 as diamonds. Despite the uncertainties introduced by the fitting procedure, the figure shows a clear trend of decrease of $r$ with lowering temperature.

This temperature dependence can be rationalized in the framework of the inhomogeneous ground state model. Let us

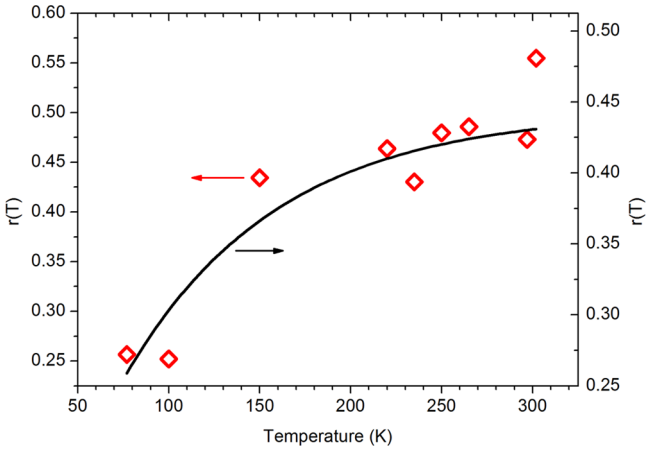


**Figure 5.** Diamonds: $r$ parameter (ratio of S* to $S_1$ ESA integrated spectra as retrieved from the SADS in Figure 4) as a function of temperature. Solid line: fit with the Boltzmann distribution described in the text.

consider two ground state isomers, named $S_0$ (the low-energy global minimum) and $S_0$* (the thermally activated local minimum at an energy higher by $\Delta E$) as in Figure 3b. Following the Boltzmann statistics, at a given temperature, the total population $N_{tot}$ will be found partially in $S_0$, with population $N_0(T) = N_{tot}/(1 + \exp(-\Delta E/k_BT))$, and partially in $S_0$*, with population $N_0^*(T) = ((N_{tot}\exp(-\Delta E/k_BT))/(1 + \exp(-\Delta E/k_BT))) = N_0(T)\exp(-\Delta E/k_BT)$. Assuming that transitions starting from the global minimum $S_0$ populate the $S_1$ state, while those starting from the higher energy isomer $S_0$* populate S* (see Figure 4b), we can write

$$r(T) = \frac{\int ESA_{S*}(\lambda, T)d\lambda}{\int ESA_{S1}(\lambda, T)d\lambda} = \frac{\int \sigma_{S*}(\lambda)N_0^*(T)d\lambda}{\int \sigma_{S1}(\lambda)N_0(T)d\lambda}$$
$$= \left[\frac{\int \sigma_{S*}(\lambda)d\lambda}{\int \sigma_{S1}(\lambda)d\lambda}\right]\frac{N_0^*(T)}{N_0(T)} = \left[\frac{\int \sigma_{S*}(\lambda)d\lambda}{\int \sigma_{S1}(\lambda)d\lambda}\right]$$
$$\times \exp(-\Delta E/k_BT)$$

where $\sigma_{S*}(\lambda)$ and $\sigma_{S1}(\lambda)$ are the (temperature-independent) ESA cross-sections for S* and $S_1$, respectively. Given that these values are unknown, we fit only the shape of $r(T)$ and scale the amplitude to match the experimentally retrieved values. The result, shown in Figure 5 as a solid line, is in very good agreement with the experimental data and allows us to retrieve a value of $\Delta E$ = 0.68 kJ/mol (which is the only free parameter in the fitting procedure).

In order to determine the nature of the two isomers, we conducted a quantum chemical analysis of spirilloxanthin, similar to a previous work on $\beta$-carotene.[27] The structural study of the investigated molecule started with the structure where the mutual orientation of the lateral parts is $\Theta_1 = \Theta_2 = 244°$. This structure belongs to the $C_2$ symmetry point group, and the dihedral angle(s) $\Theta_{1(2)}$ is the dihedral angle defined between bonds 1, 2, 3 or 1′, 2′, 3′, respectively, as indicated in Figure 1. In Figure 6, we show the one-dimensional B3LYP/SV(P) potential energy cut for a fixed angle $\Theta_1 = 244°$ and variation of $\Theta_2$. We retrieve two minima at 119° and 244° and two maxima at $\Theta_2 = 178°$ and planar arrangements ($\Theta_2 = 0/360°$). As can be seen in Figure 6, the lowest energy barriers between two minimum-energy conformations are 9.8 kJ·mol$^{-1}$ (from the $S_0$-


dx.doi.org/10.1021/jp4011372 | J. Phys. Chem. A 2013, 117, 6303−6310

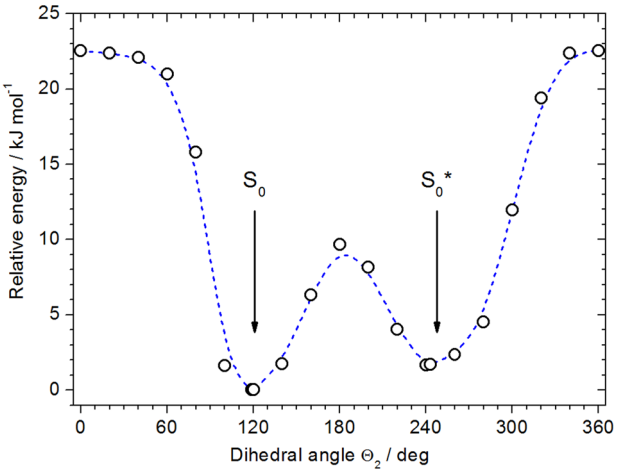


**Figure 6.** One dimensional B3LYP/SV(P) torsional potential for the electronic ground state for $\Theta_1$ = 244° and variation of $\Theta_2$. The corresponding $S_0$ and $S_0$* ground states are also indicated.

minimum) and/or 8.0 kJ·mol$^{-1}$ (from the $S_0$* minimum). The barrier heights at planar arrangements are approximately two-times larger, i.e., 22.5/20.9 kJ mol$^{-1}$.

According to previously published works on carotenoids,[27,54,55] TD-DFT fails to predict the energy of the lowest lying singlet state $S_1$ with negligible oscillator strength due to its doubly excited character. In the case of the investigated symmetric conformation for $\Theta_2$ = 244°, our TD-B3LYP//B3LYP/SV(P) and/or TD-BHLYP//BHLYP/SV(P) calculations show that the lowest optically allowed vertical transition energy to the first excited state of $1^1$B symmetry is 2.097 eV (B3LYP) and 2.434 eV (BHLYP) respectively, with large oscillator strengths of 6.99 (B3LYP) and 6.67 (BHLYP). Comparison with the experimental value[30] of 2.34 (measured in acetone) or 2.18 eV (measured in $CS_2$) shows that the gas-phase TD-B3LYP energy is blue-shifted and the TD-BHLYP energy is red-shifted. The next two calculated optical transitions have very small oscillator strengths.

The dominating electronic transition is connected with the excitation from the highest occupied molecular orbital (HOMO) to the lowest unoccupied molecular orbital (LUMO). The HOMO orbital is regularly delocalized over the carbon−carbon double bonds between the outer methyl groups of the polyenic chain (see Figure 7). Its irreducible representation is A. However, the LUMO orbital is delocalized over the single C−C bonds. Its irreducible representation is B. The HOMO to LUMO transition with 96% contribution dominates in this optically allowed vertical transition. The second transition of $2^1$A symmetry comes from the HOMO to LUMO+1 and HOMO−1 to LUMO orbitals. In this case, the LUMO+1 and HOMO−1 orbitals are symmetrically split over bonds connected with the methyl groups on the polyenic chain. The third optical transition of $2^1$B symmetry is connected mainly with the HOMO−2 to LUMO orbitals. The correct order of optical transitions with respect to the oscillator strength can be obtained using the multireference ab initio calculations. As indicated in Table 2, both conformations exhibit one forbidden transition at 3.4 eV for CAS-SCF method and two forbidden transitions for MRCI method at 1.8 and 2.0 eV.

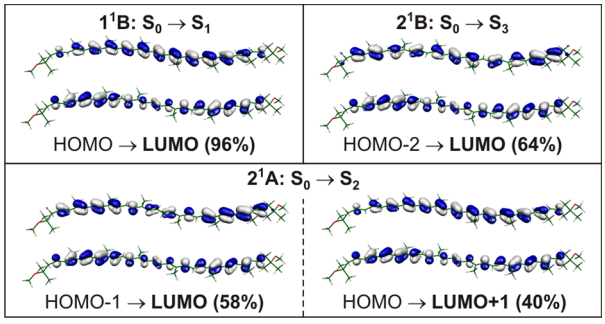


**Figure 7.** Plots of the B3LYP molecular orbitals significantly contributing to the TD-B3LYP lowest energy transitions of the symmetric conformation ($\Theta_1$ = $\Theta_2$ = 244°). The values in parentheses stand for percentages of the excitation contributions in individual transitions. The value of the depicted isosurface is 0.03 in bohr$^{-3/2}$.

The value of the energy difference $\Delta E$ of 1.68 kJ mol$^{-1}$ between the local and the global minimum is considerably higher than the value of 0.68 kJ/mol obtained from the fit to the experimental data in Figure 5. One obvious reason for this difference is that, in the fit in Figure 5, the ratio between the transition strengths of $S_1$ and S* is unknown and was scaled arbitrarily. Knowledge of this factor might change the value obtained for $\Delta E$. Another factor explaining the discrepancy to the B3LYP/SV(P) calculations is the neglect of solvent effects. Consideration of solute−solvent interactions might alter the potential curve in Figure 6 drastically.

## DISCUSSION

Ground state conformers of carotenoids have been employed by several groups to explain ultrafast spectroscopic measurements. In an investigation of light harvesting complex 1, Papagiannakis et al.[26] discussed the intensity dependence of S* in terms of two molecular ensembles with different transition dipole moments from the electronic ground state. Such a possibility was disregarded by the same authors in favor of a so-called two photon model, involving an excited state transition in the visible from $S_2$ to $S_{n,2}$. Recently, Kosumi et al.[32] conducted an intensity dependent study of spirilloxanthin in solution and as part of a light harvesting complex. In agreement with Papagiannakis et al., Kosumi et al. found that the intensity dependences of $S_1$ and S* are similar and therefore ruled out the involvement of different ground conformers as they would need similar ground state transition dipole moments in order to exhibit the same intensity dependent behavior. Our quantum chemical calculations, however, show that the transition dipole moments $\mu$ for the global and the local minimum in Figure 6 are equal down to a level of 0.2% (see Table 2, CAS-SCF results). This makes it unfeasible to distinguish them in an intensity dependent study.

The inhomogeneous ground state model does not only explain the temperature dependence of the S*/$S_1$ ratio discussed in Figure 5. The model also rationalizes the shape of the bleaching signal after decay of $S_1$.[31,32] The GSB signal after the depopulation of $S_1$ but before the decay of S* is more structured than the absorption spectrum or the GSB signal within the $S_1$-lifetime. Chabera et al.[31] invoked a planar ground-state subpopulation as the source of S* to explain their findings. The higher lying symmetric minimum in Figure 6 is an ideal candidate for such a planar local minimum, as it is closer to $C_{2h}$ symmetry than the more twisted lower lying minimum at $\Theta_2$ = 119°. The same conclusions were drawn from a quantum chemical study on $\beta$-carotene.[27]


dx.doi.org/10.1021/jp4011372 | J. Phys. Chem. A 2013, 117, 6303−6310

Table 2. TD-DFT/SVP//B3LYP/SV(P) or ab Initio CAS-SCF//B3LYP/SV(P) and MRCI//B3LYP/SV(P) Vertical Excitation Energies for the Conformations of the Studied Molecules ($\Theta_1$ = 244°); the Values in Parentheses Are the Oscillator Strengths

| $\Theta_2$ | | $S_0 \rightarrow S_1$ | $S_0 \rightarrow S_2$ | $S_0 \rightarrow S_3$ |
|---|---|---|---|---|
| 119° | TD-B3LYP | 2.098 eV or 16918 $cm^{-1}$ (7.00313) | 2.260 eV or 18226 $cm^{-1}$ (0.00084) | 2.856 eV or 23039 $cm^{-1}$ (0.28994) |
| | TD-BHLYP | 2.437 eV or 19645 $cm^{-1}$ (6.67245) | 3.268 eV or 26355 $cm^{-1}$ (0.00008) | 3.634 eV or 29306 $cm^{-1}$ (0.00075) |
| | CAS-SCF | 3. 441 eV or 27755 $cm^{-1}$ (0.00011) | 3.819 eV or 30794 $cm^{-1}$ (5.21545) | 4.258 eV or 34339 $cm^{-1}$ (0.10625) |
| | MRCI | 1.798 eV or 14497 $cm^{-1}$ (0.00000) | 1.967 eV or 15860 $cm^{-1}$ (0.00001) | 2.742 eV or 22109 $cm^{-1}$ (5.00702) |
| 244° | TD-B3LYP | 2.097 eV or 16914 $cm^{-1}$ (6.98647) | 2.259 eV or 18219 $cm^{-1}$ (0.00033) | 2.856 eV or 23033 $cm^{-1}$ (0.29671) |
| | TD-BHLYP | 2.434 eV or 19631 $cm^{-1}$ (6.66884) | 3.261 eV or 26298 $cm^{-1}$ (0.00380) | 3.635 eV or 29313 $cm^{-1}$ (0.00876) |
| | CAS-SCF | 3. 440 eV or 27742 $cm^{-1}$ (0.00002) | 3. 822 eV or 30825 $cm^{-1}$ (5.19703) | 4.264 eV or 34388 $cm^{-1}$ (0.10795) |
| | MRCI | 1.831 eV or 14768 $cm^{-1}$ (0.00001) | 2.050 eV or 16535 $cm^{-1}$ (0.00006) | 2.757 eV or 22230 $cm^{-1}$ (5.06185) |

We note that excited state isomers as discussed by Niedzwiedzki et al.[21,30] are less suited for explaining temperature-dependent effects on the amplitude of S*: if the isomers are assumed to be formed on $S_1$ rather than on $S_0$, they would be populated with an excess energy defined by the energy difference between $S_2$ and $S_1$, not by thermal excess energy as for ground state isomers. A decrease in temperature should therefore only affect ground and not excited state isomers.

## CONCLUSIONS AND OUTLOOK

In this work, we systematically investigated the temperature dependence of S* in relation to $S_1$ in spirilloxanthin. The PMMA matrix provides a similar environment at both RT and 77 K. We see a clear trend of decreasing $S^*/S_1$ ratio as the temperature is lowered. This trend follows roughly a Boltzmann distribution, adding further proof to the concept of an inhomogeneous ground state in spirilloxanthin: $S_1$ is formed by an energetically lower-lying isomer, while S* is the lowest-lying singlet state of a local minimum on the electronic ground state. This hypothesis is experimentally corroborated by the fact that the S* signal can be frozen out. We consider this model to be general, not limited to spirilloxanthin but applicable to all carotenoids with an S* signal. As determined by the low energy barrier between the minima in Figure 6, the rate of exchange between the two isomers is in the nanosecond time range,[27] which makes attempts to chemically purify the sample unfeasible. In order to explain pump−deplete−probe results[22] within the framework of the inhomogeneous ground state model, the two isomers are expected to exhibit different $S_2$ spectra in the NIR region. Specifically, a 1000 nm depletion pulse was shown to selectively deplete $S_1$ but not S*. Therefore, we expect the $S_1$-forming $S_2$ state to absorb more strongly in this region with respect to the $S_2$* state (see Figure 3b). Such a pump−NIR−probe experiment at different temperatures is the subject of ongoing investigations.

## AUTHOR INFORMATION


### Corresponding Author

*(D.P.) E-mail: dario.polli@polimi.it.

### Author Contributions

⊥These authors contributed equally to this work.


### Notes

The authors declare no competing financial interest.

## ACKNOWLEDGMENTS

D.P., R.J.C., and S.H. acknowledge financial support by the Human Frontiers Science Program Grant Number RGP0005. G.C. acknowledges support by the European Research Council Advanced Grant STRATUS (ERC-2011-AdG No. 291198). J.H. and G.C. are grateful for the financial support by LASERLAB-EUROPE (grant agreement no. 284464, EC's Seventh Framework Programme). J.H. acknowledges funding by the Austrian Science Fund (FWF): START project Y 631-N27. A.M.C. was supported as a part of the Photosynthetic Antenna Research Center (PARC), an Energy Frontier Research Center funded by the DOE, Office of Science, Office of Basic Energy Sciences under Award Number DE-SC 0001035. Carotenoid samples were prepared by A.M.C.

## REFERENCES


(1) Polivka, T.; Sundstrom, V. Ultrafast Dynamics of Carotenoid Excited States: from Solution to Natural and Artificial Systems. *Chem. Rev.* **2004**, *104*, 2021−2071.

(2) Polivka, T.; Sundstrom, V. Dark Excited States of Carotenoids: Consensus and Controversy. *Chem. Phys. Lett.* **2009**, *477*, 1−11.

(3) Cerullo, G.; Polli, D.; Lanzani, G.; De Silvestri, S.; Hashimoto, H.; Cogdell, R. J. Photosynthetic Light Harvesting by Carotenoids: Detection of an Intermediate Excited State. *Science* **2002**, *298*, 2395−2398.

(4) McCamant, D. W.; Kukura, P.; Mathies, R. A. Femtosecond Time-Resolved Stimulated Raman Spectroscopy: Application to the Ultrafast Internal Conversion in Beta-Carotene. *J. Phys. Chem. A* **2003**, *107*, 8208−8214.

(5) Hauer, J.; Buckup, T.; Motzkus, M. Pump-Degenerate Four Wave Mixing As a Technique for Analyzing Structural and Electronic Evolution: Multidimensional Time-Resolved Dynamics near a Conical Intersection. *J. Phys. Chem. A* **2007**, *111*, 10517−10529.

(6) Marek, M. S.; Buckup, T.; Motzkus, M. Direct Observation of a Dark State in Lycopene Using Pump-Dfwm. *J. Phys. Chem. B* **2011**, *115*, 8328−8337.

(7) Sugisaki, M.; Fujiwara, M.; Kosumi, D.; Fujii, R.; Nango, M.; Cogdell, R. J.; Hashimoto, H. Comparison of Transient Grating Signals from Spheroidene in an Organic Solvent and in Pigment−Protein Complexes from Rhodobacter Sphaeroides 2.4.1. *Phys. Rev. B* **2010**, *81*, 245112.

(8) Buckup, T.; Hauer, J.; Mohring, J.; Motzkus, M. Multidimensional Spectroscopy of Beta-Carotene: Vibrational Cooling in the Excited State. *Arch. Biochem. Biophys.* **2009**, *483*, 219−223.

(9) Hauer, J.; Skenderovic, H.; Kompa, K. L.; Motzkus, M. Enhancement of Raman Modes by Coherent Control in Beta-Carotene. *Chem. Phys. Lett.* **2006**, *421*, 523−528.

(10) Christensson, N.; Polivka, T.; Yartsev, A.; Pullerits, T. Photon Echo Spectroscopy Reveals Structure-Dynamics Relationships in Carotenoids. *Phys. Rev. B* **2009**, *79*, 245118.

(11) Christensson, N.; Milota, F.; Nemeth, A.; Sperling, J.; Kauffmann, H. F.; Pullerits, T.; Hauer, J. Two-Dimensional Electronic Spectroscopy of Beta-Carotene. *J. Phys. Chem. B* **2009**, *113*, 16409−16419.

(12) Christensson, N.; Milota, F.; Nemeth, A.; Pugliesi, I.; Riedle, E.; Sperling, J.; Pullerits, T.; Kauffmann, H.; Hauer, J. Electronic Double-Quantum Coherences and Their Impact on Ultrafast Spectroscopy: The Example of Beta-Carotene. *J. Phys. Chem. Lett.* **2010**, *1*, 3366−3370.

(13) Calhoun, T. R.; Davis, J. A.; Graham, M. W.; Fleming, G. R. The Separation of Overlapping Transitions in Beta-Carotene with Broadband 2d Electronic Spectroscopy. *Chem. Phys. Lett.* **2012**, *523*, 1−5.
(14) Andersson, P. O.; Gillbro, T. Photophysics and Dynamics of the Lowest Excited Singlet-State in Long Substituted Polyenes with Implications to the Very Long-Chain Limit. *J. Chem. Phys.* **1995**, *103*, 2509−2519.
(15) Polivka, T.; Balashov, S. P.; Chabera, P.; Imasheva, E. S.; Yartsev, A.; Sundstrom, V.; Lanyi, J. K. Femtosecond Carotenoid to Retinal Energy Transfer in Xanthorhodopsin. *Biophys. J.* **2009**, *96*, 2268−2277.
(16) Amarie, S.; Lupo, D.; Lenz, M. O.; Saegesser, R.; Ghosh, R.; Wachtveitl, J. Excitation Energy Pathways in the Photosynthetic Units of Reaction Center Lm- and H-Subunit Deletion Mutants of Rhodospirillum Rubrum. *Photosynth. Res.* **2010**, *103*, 141−151.
(17) Papagiannakis, E.; Kennis, J. T. M.; van Stokkum, I. H. M.; Cogdell, R. J.; van Grondelle, R. An Alternative Carotenoid-to-Bacteriochlorophyll Energy Transfer Pathway in Photosynthetic Light Harvesting. *Proc. Natl. Acad. Sci. U.S.A.* **2002**, *99*, 6017−6022.
(18) Larsen, D. S.; Papagiannakis, E.; Vengris, M.; Valkunas, L.; Cogdell, R. J.; van Grondelle, R. Excited-State Dynamics of Carotenoids in Light-Harvesting Complexes. 2. Dissecting Pulse Structures from Optimal Control Experiments. *J. Phys. Chem. B* **2006**, *110*, 5737−5746.
(19) Jailaubekov, A. E.; Vengris, M.; Song, S. H.; Kusumoto, T.; Hashimoto, H.; Larsen, D. S. Deconstructing the Excited-State Dynamics of Beta-Carotene in Solution. *J. Phys. Chem. A* **2011**, *115*, 3905−3916.
(20) Berera, R.; van Stokkum, I. H. M.; Kodis, G.; Keirstead, A. E.; Pillai, S.; Herrero, C.; Palacios, R. E.; Vengris, M.; van Grondelle, R.; Gust, D.; Moore, T. A.; Moore, A. L.; Kennis, J. T. M. Energy Transfer, Excited-State Deactivation, and Exciplex Formation in Artificial Caroteno-Phthalocyanine Light-Harvesting Antennas. *J. Phys. Chem. B* **2007**, *111*, 6868−6877.
(21) Niedzwiedzki, D. M.; Sullivan, J. O.; Polivka, T.; Birge, R. R.; Frank, H. A. Femtosecond Time-Resolved Transient Absorption Spectroscopy of Xanthophylls. *J. Phys. Chem. B* **2006**, *110*, 22872−22885.
(22) Buckup, T.; Savolainen, J.; Wohlleben, W.; Herek, J. L.; Hashimoto, H.; Correia, R. R. B.; Motzkus, M. Pump-Probe and Pump-Deplete-Probe Spectroscopies on Carotenoids with $N$ = 9−15 Conjugated Bonds. *J. Chem. Phys.* **2006**, *125*, 194505.
(23) Savolainen, J.; Buckup, T.; Hauer, J.; Jafarpour, A.; Serrat, C.; Motzkus, M.; Herek, J. L. Carotenoid Deactivation in an Artificial Light-Harvesting Complex Via a Vibrationally Hot Ground State. *Chem. Phys.* **2009**, *357*, 181−187.
(24) Lenzer, T.; Ehlers, F.; Scholz, M.; Oswald, R.; Oum, K. Assignment of Carotene S* State Features to the Vibrationally Hot Ground Electronic State. *Phys. Chem. Chem. Phys.* **2010**, *12*, 8832−8839.
(25) Golibrzuch, K.; Ehlers, F.; Scholz, M.; Oswald, R.; Lenzer, T.; Oum, K.; Kim, H.; Koo, S. Ultrafast Excited State Dynamics and Spectroscopy of 13,13′-Diphenyl-Beta-Carotene. *Phys. Chem. Chem. Phys.* **2011**, *13*, 6340−6351.
(26) Papagiannakis, E.; van Stokkum, I. H. M.; Vengris, M.; Cogdell, R. J.; van Grondelle, R.; Larsen, D. S. Excited-State Dynamics of Carotenoids in Light-Harvesting Complexes. 1. Exploring the Relationship between $S_1$ and S* States. *J. Phys. Chem. B* **2006**, *110*, 5727−5736.
(27) Lukes, V.; Christensson, N.; Milota, F.; Kauffmann, H.; Hauer, J. Electronic Ground State Conformers of Beta-Carotene and Their Role in Ultrafast Spectroscopy. *Chem. Phys. Lett.* **2011**, *506*, 122−127.
(28) Ostroumov, E. E.; Muller, M. G.; Reus, M.; Holzwarth, A. R. On the Nature of the "Dark S*" Excited State of Beta-Carotene. *J. Phys. Chem. A* **2011**, *115*, 3698−3712.
(29) Jailaubekov, A. E.; Song, S. H.; Vengris, M.; Cogdell, R. J.; Larsen, D. S. Using Narrowband Excitation to Confirm That the S* State in Carotenoids Is Not a Vibrationally-Excited Ground State Species. *Chem. Phys. Lett.* **2010**, *487*, 101−107.
(30) Niedzwiedzki, D.; Koscielecki, J. F.; Cong, H.; Sullivan, J. O.; Gibson, G. N.; Birge, R. R.; Frank, H. A. Ultrafast Dynamics and Excited State Spectra of Open-Chain Carotenoids at Room and Low Temperatures. *J. Phys. Chem. B* **2007**, *111*, 5984−5998.
(31) Chabera, P.; Fuciman, M.; Hribek, P.; Polivka, T. Effect of Carotenoid Structure on Excited-State Dynamics of Carbonyl Carotenoids. *Phys. Chem. Chem. Phys.* **2009**, *11*, 8795−8803.
(32) Kosumi, D.; Maruta, S.; Horibe, T.; Nagaoka, Y.; Fujii, R.; Sugisaki, M.; Cogdell, R. J.; Hashimoto, H. Ultrafast Excited State Dynamics of Spirilloxanthin in Solution and Bound to Core Antenna Complexes: Identification of the S* and T-1 States. *J. Chem. Phys.* **2012**, *137*, 064505.
(33) Bose, S. K.; Gest, H. Bacterial Photophosphorylation: Regulation by Redox Balance. *Proc. Natl. Acad. Sci. U.S.A.* **1963**, *49*, 337−345.
(34) Gardiner, A. T.; Cogdell, R. J.; Takaichi, S. The Effect of Growth-Conditions on the Light-Harvesting Apparatus in Rhodopseudomonas-Acidophila. *Photosynth. Res.* **1993**, *38*, 159−167.
(35) Nakagawa, K.; Suzuki, S.; Fujii, R.; Gardiner, A. T.; Cogdell, R. J.; Nango, M.; Hashimoto, H. Probing Binding Site of Bacteriochlorophyll a and Carotenoid in the Reconstituted Lh1 Complex from Rhodospirillum Rubrum S1 by Stark Spectroscopy. *Photosynth. Res.* **2008**, *95*, 339−344.
(36) Manzoni, C.; Polli, D.; Cerullo, G. Two-Color Pump-Probe System Broadly Tunable over the Visible and the near Infrared with Sub-30 Fs Temporal Resolution. *Rev. Sci. Instrum.* **2006**, *77*, 023103.
(37) Polli, D.; Luer, L.; Cerullo, G. High-Time-Resolution Pump-Probe System with Broadband Detection for the Study of Time-Domain Vibrational Dynamics. *Rev. Sci. Instrum.* **2007**, *78*, 103108.
(38) van Stokkum, I. H. M.; Larsen, D. S.; van Grondelle, R. Global and Target Analysis of Time-Resolved Spectra. *Biochim. Biophys. Acta, Bioenerg.* **2004**, *1658*, 262−262.
(39) Lee, C. T.; Yang, W. T.; Parr, R. G. Development of the Colle−Salvetti Correlation-Energy Formula into a Functional of the Electron-Density. *Phys. Rev. B* **1988**, *37*, 785−789.
(40) Becke, A. D. A New Mixing of Hartree−Fock and Local Density-Functional Theories. *J. Chem. Phys.* **1993**, *98*, 1372−1377.
(41) Furche, F.; Ahlrichs, R. Adiabatic Time-Dependent Density Functional Methods for Excited State Properties. *J. Chem. Phys.* **2002**, *117*, 7433−7447.
(42) Jensen, F. *Introduction to Computational Chemistry*; John Wiley and Sons: Chichester, U.K., 2007.
(43) Gdanitz, R. J.; Ahlrichs, R. The Averaged Coupled-Pair Functional (ACPF): A Size-Extensive Modification of MR CI(SD). *Chem. Phys. Lett.* **1988**, *143*, 413−420.
(44) Becker, U.; Bykov, D.; Ganyushin, D.; Hansen, A.; Izsak, R.; Liakos, G.; Kollmar, C.; Kossmann, S.; Pantazis, D. A.; Petrenko; et al. *ORCA*, program version 2.9.1 release; Max-Planck-Institute for Bioinorganic Chemistry: Mülheim a.d.Ruhr, Germany, 2012.
(45) Dunning, T. H.; Harrison, P. J. *Modern Theoretical Chemistry*; Plenum Press: New York, 1977; Vol. 2.
(46) Dunning, T. H.; Hay, P. J. *Methods of Electronic Structure Theory*; Plenum Press: New York, 1977; Vol. 2.
(47) Lukes, V.; Aquino, A. J. A.; Lischka, H.; Kauffmann, H. F. Dependence of Optical Properties of Oligo-Para-Phenylenes on Torsional Modes and Chain Length. *J. Phys. Chem. B* **2007**, *111*, 7954−7962.
(48) Beenken, W. J. D. Torsional Broadening in Absorption and Emission Spectra of Bithiophene As Calculated by Time-Dependent Density Functional Theory. *Chem. Phys.* **2008**, *349*, 250−255.
(49) Lukes, V.; Aquino, A. J. A.; Lischka, H. Theoretical Study of Vibrational and Optical Spectra of Methylene-Bridged Oligofluorenes. *J. Phys. Chem. A* **2005**, *109*, 10232−10238.
(50) Fujii, R.; Inaba, T.; Watanabe, Y.; Koyama, Y.; Zhang, J. P. Two Different Pathways of Internal Conversion in Carotenoids Depending on the Length of the Conjugated Chain. *Chem. Phys. Lett.* **2003**, *369*, 165−172.

(51) Nishimura, K.; Rondonuwu, F. S.; Fujii, R.; Akahane, J.; Koyama, Y.; Kobayashi, T. Sequential Singlet Internal Conversion of $1B_u^+ \rightarrow 3A_g^- \rightarrow 1B_u^- \rightarrow 2A_g^- \rightarrow (1A_g^-$ Ground) in All-Trans-Spirilloxanthin Revealed by Two-Dimensional Sub-5-fs Spectroscopy. *Chem. Phys. Lett.* **2004**, *392*, 68−73.
(52) Gradinaru, C. C.; Kennis, J. T. M.; Papagiannakis, E.; van Stokkum, I. H. M.; Cogdell, R. J.; Fleming, G. R.; Niederman, R. A.; van Grondelle, R. An Unusual Pathway of Excitation Energy Deactivation in Carotenoids: Singlet-to-Triplet Conversion on an Ultrafast Timescale in a Photosynthetic Antenna. *Proc. Natl. Acad. Sci. U.S.A.* **2001**, *98*, 2364−2369.
(53) May, V.; Kuehn, O. *Charge and Energy Transfer Dynamics in Molecular Systems*, 3rd ed.; WILEY-VCH Verlag GmbH: Weinheim, Germany, 2011.
(54) Holzwarth, A. R.; Ostroumov, E. E.; Muller, M. G.; Hundsdorfer, C.; Stahl, W.; Marian, C. M. Excited State Relaxation Dynamics and Electronic Properties of a Quinoid Carotenoid. *Chem. Phys.* **2010**, *373*, 137−144.
(55) Marian, C. M.; Kock, S. C.; Hundsdorfer, C.; Martin, H. D.; Stahl, W.; Ostroumov, E.; Muller, M. G.; Holzwarth, A. R. Spectroscopic Properties of Phenolic and Quinoid Carotenoids: A Combined Theoretical and Experimental Study. *Photochem. Photobiol. Sci.* **2009**, *8*, 270−278.